Investigating PAI-1, ICAM-1, and VCAM-1 expression dependence on neural activity within the acute phase of stroke in mice endothelial cells

by

Samuel A. Burford

A Thesis Submitted in Partial Fulfillment of the
Requirements of the Degree of

BACHELOR OF SCIENCE (HONOURS)

In the Department of Biology

University of Victoria

We acknowledge and respect the lək̓ʷəŋən peoples on whose traditional territory the university stands and the Songhees, Esquimalt and W̱SÁNEĆ peoples whose historical relationships with the land continue to this day.

Investigating PAI-1, ICAM-1, and VCAM-1 expression dependence on neural activity within the acute phase of stroke in mice endothelial cells

by

Samuel A. Burford

Supervisor Committee

Dr. Craig Brown, Supervisor
Division of Medical Sciences

Dr. Gautam Awatramani, Co-Supervisor
Department of Biology

Abstract

Stroke is a leading cause of death and disability worldwide. Following an Ischemic stroke, of which 87% of all strokes are, a spreading depolarization occurs, propagating damage to healthy tissue. Through initial experimentation, the procoagulant protein Plasminogen Activator Inhibitor-1 (PAI-1) displayed a unique expression pattern 24 hours following an ischemic stroke model in mice, producing a localized region of expression within endothelial cells contralateral to the stroke site. Through the application of a strong GABA agonist and using a passive diffusion method to limit tissue damage, my goal was to determine if the neural activity of the spreading depolarization was responsible for PAI-1 expression. I also aimed to observe expression patterns of Intracellular Adhesion Molecule-1 (ICAM-1) and Vascular Cell Adhesion Molecule-1 (VCAM-1) using immunolabelling. Expression of PAI-1 through immunolabelling was inconclusive due to high levels of endogenous binding of the secondary antibody. An attempt to limit endogenous binding was unsuccessful. VCAM-1 imaging did not display significant expression, however ICAM-1 did display a stroke dependent expression, in a pattern where proximity to the stroke site was indicative of total expression. Though PAI-1 expression manipulation was inconclusive, the potential for neural dependency in its expression remains. ICAM-1 expression results indicate a correlation between ICAM-1 expression and inflammation following stroke and likely does not display any neural activity dependence. If neural activity dependence can be further investigated in PAI-1, along with the identification of a potential neurovascular coupling pathway, then the expression of other vascular proteins may be studied to better understand the implications and reach of spreading depolarizations, along with the potential damage or resilience they may provide.

Table of Contents

List of Figures

List of Abbreviations

ATP: Adenosine Triphosphate

EC: Endothelial Cell

ICAM-1: Intracellular Adhesion Molecule-1

GABA: Gamma Aminobutyric Acid

PAI-1: Plasminogen Activator Inhibitor-1

ROS: Reactive Oxidating Species

SD: Spreading Depolarization

tPA: Tissue Plasminogen Activator

uPA: Urokinase Plasminogen Activator

VCAM-1: Vascular Cell Adhesion Molecule-1

Acknowledgements

I would first like to thank Dr. Brown for the opportunity to begin my journey into academic research and for guidance throughout the project. I would like to thank Dr. Awatramani for co-supervision, Dr. Nashmi for acting as an external examiner, and Dr. Chow and Dr. Hawkins for their support as honours advisors. I would also like to thank the Animal Care Services for their dedication to academic research, along with their training and support.

I am incredibly grateful to be a part of the Brown Lab, where I have met many colleagues and many more friends. Without the constant support, teaching, and advice from my lab peers, none of this work would have been possible. Pat, Sorabh, Dominique, Taylor, Tanaka, Vasil, Jenna, Myrthe, Dhwani, Frances, Ana Paula, Emilie, and Adam, I thank you all! A special thank you to Kamal, who initiated this research topic and whose guidance is the sole reason this work has reached a final product.

I would also like to extend a huge thank you to all my supportive undergraduate friends. You have all brought me to where I am today. Meike, Thea, Johnny, Simi, Riya, Katerina, Emir, Oliver, and Miriam, I thank you all!

Finally, I would like to thank my family for the continued support throughout my everyday life and education. I am incredibly fortunate to be where I am today.

"Tell me with whom you associate, and I will tell you who you are."
-Johann Wolfgang von Goethe

Introduction

Ischemic Stroke

In Canada, over 100,000 strokes occur each year resulting in hospitalization or need for emergency services (Holodinsky *et al.*, 2022). Stroke occurrence is increasing both globally and in Canada, where it is estimated a stroke event occurs every 5 minutes. Furthermore, the cost of stroke is extensive, costing the United States $56 billion annually, over $36 billion of which is direct medical cost (Tsao *et al.*, 2023). The average patient loses approximately 1.9 million neurons per minute in an untreated stroke (Saver, 2006), leading to a wide range of symptoms and structural brain damage. Considering the current data, stroke remains a devastating disease that affects millions worldwide each year and is a leading cause of both death and disability. Further understanding of how the brain reacts following a stroke is essential, allowing for a greater development and implementation of therapeutic treatments.

When a blockage occurs within a blood vessel, leading to a loss of blood flow to a region of brain tissue, it is termed an ischemic stroke. This primarily affected region of neural tissue, known as the infarct zone, undergoes neuronal death due to a deprivation of glucose and oxygen supply (Obeidat *et al.*, 2000). The infarct region is considered irreversible damage, however the surrounding area, known as the peri infarct, grows as time passes. If treatment can occur rapidly, then a greater percentage of the peri infarct region can be saved. This is why a rapid response to stroke is crucial in the discussion of stroke recovery (Saver, 2006).

87% of all strokes are ischemic strokes (Tsao et al., 2023), with the remaining 13% being hemorrhagic strokes. Hemorrhagic strokes occur when a blood vessel bursts, limiting blood flow

to the infarct region as blood escapes the blood vessels. This can occur due to high blood pressure straining a weakened blood vessel, or head trauma. Alternatively, treatment of an ischemic stroke can cause what is known as hemorrhagic transformation, where in a therapeutic attempt to remove a blood clot sourcing an ischemic stroke, a hemorrhagic stroke occurs (Hong *et al.,* 2021; Ribo *et al*., 2004). This can often be a fatal complication.

The mouse stroke model used in this research was a photothrombotic stroke, in which a reactive dye in the bloodstream becomes activated by the shining of a particular wavelength (see Photothrombotic Stroke in methods, Watts *et al.,* 2015). This model is comparatively less invasive than other stroke models, with lower mortality rates, and activates a very similar cascade of damage to that of a real stroke (Barthels and Das, 2018). Furthermore, precise localization of the infarct region allows for region-specific research in response to stroke. The largest discrepancy between the model and reality is the clotting pattern. The photothrombotic model produces clotting throughout the capillary bed. An ischemic stroke would instead produce a clot within an upstream blood vessel, limiting blood flow to the capillaries through a single clot instead of multiple smaller clots. Taken together, the photothrombotic stroke model is an effective research tool in stroke recovery and treatment.

Spreading Depolarizations

The cause of damage propagation from the infarct region to the peri infarct region, as well as more distal regions of the brain, has been called into question in recent years. The long-standing explanation for this affect has been the glutamate excitotoxicity theory, where an increase in glutamate travels along grey matter tracts to impact other regions of the brain. However, new

research is supportive of a different model, in which ischemic spreading depressions, or spreading depolarizations (SD) (Leao, 1947), are responsible for the exacerbation of damage initially caused by loss of glucose and oxygen supply (Andrew *et al.*, 2022). A SD is produced by a broad increase in neuron membrane potentials, increasing from their usual resting negative potential to ~ 0mV (Czeh *et al.,* 1993). A lack of blood supply and oxygen leads to a deficit of Adenosine Triphosphate (ATP), halting the activity of sodium/potassium ATPase pumps, which are crucial for the maintenance of a negative resting potential. This loss of membrane potential has been shown to induce swelling in neural cells, spreading to healthy regions of the brain (Hellas and Andrew, 2021). This spread can occur rapidly, within 20 minutes of blood supply loss and spreading up to 9mm/min along grey matter (Drier *et al*., 2017). Work has been done to determine ways to inhibit the effect of SDs, however more research is required to fully understand the effects, spread, and underlying mechanism.

PAI-1

Following a stroke event, the brain adapts by making many physical and genetic alterations. In a recent study by Callegari *et al*. (2023), alterations within a mouse model stroke were compared to non-fatal human strokes. Of the genetic changes observed, one of the most coordinated changes between both mouse and human was an increase in *Serpine1* expression. *Serpine1* is the gene that encodes for the protein Plasminogen Activator Inhibitor-1 (PAI-1). PAI-1 plays a vital role in the plasminogen/plasmin system, where it acts as a procoagulant by inhibiting tissue Plasminogen Activator (tPA) and urokinase Plasminogen Activator (uPA) (Figure 1.) (Sillen and Declerck, 2021). This leads to the inhibition of fibrinolysis and persistence of fibrin clots.

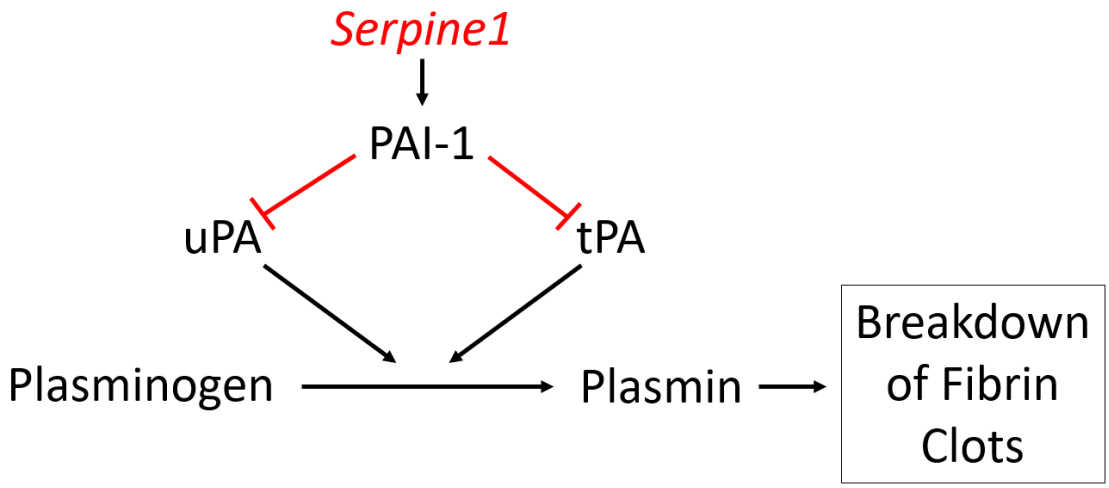

Figure 1. Summary of PAI-1's role in the inhibition of fibrinolysis. Figure adapted from Sillen and Dicklerck (2021). PAI-1's direct inhibition of tissue Plasminogen Activator (tPA) and urokinase Plasminogen Activator (uPA) allows for coagulation to persist and the retention of fibrin clots.

At a first approximation, the upregulation of *Serpine1* following stroke seems counterintuitive. Ischemic stroke is caused by a blockage and the promotion of a procoagulant would only further hinder the ability to remove the blockage and re-perfuse neuronal tissue. Furthermore, tPA, which is directly inhibited by PAI-1, is currently the most accessible and common acute treatment for stroke, in which tPA is administered to suitable patients within 4.5 hours of the development of an ischemic stroke, known as intravenous thrombolysis (The National Institute of Neurological Disorders and Stroke rt-PA Stroke Study Group, 1994; Desai and Smith, 2013).

From an evolutionary perspective, the increase in *Serpine1* may be justified. Major risk factors for ischemic stroke, such as smoking and obesity (George, 2020) have only been prominent for a short period of time throughout human history, whereas hemorrhagic strokes from head trauma have likely been present for hundreds of thousands of years. It is possible that the expression of *Serpine1* is an artifact of procoagulant expression following a hemorrhagic stroke. However, *Serpine1*'s expression of PAI-1 does appear to provide secondary benefits to neural function. The

increased presence of PAI-1 protein has been shown to promote the recruitment of microglia and phagocytotic activity when sourced from microglia (Jeon *et al*., 2012). Research has also indicated that PAI-1 may play a role in mitigating neurotoxicity (Cho *et al.*, 2012; Docagne *et al*., 2002) and anti-apoptotic signalling (Soeda *et al*., 2008). As for the mechanism of *Serpine1* increase following stroke, the presence of reactive oxidating species (ROS) and pro-inflammatory signalling promote the *Serpine1* expression (Rahman and Krause, 2020), both of which are prominent following stroke. Pro-fibrotic signalling and hormonal signalling are also capable of increasing *Serpine1*, responding to signalling cues such as angiotensin-II and insulin (Vaughan *et al.,* 1995).

Initial PAI-1 Expression Findings

In a pilot study performed within our laboratory, it was determined that 3 days following a photothrombotic stroke model in mice (see methods for further details) widespread expression of PAI-1 was observed within endothelial cells (EC) (Figure 2a,b). EC's make up the walls of blood vessels and are the only cells that fully encapsulate the capillaries found within the brain. This immunolabelling timeframe aligns with the increase in *Serpine1* expression observed following stroke from other studies, as well as RNA data from our lab tracking mature RNA to determine the expression of *Serpine1* that will encode PAI-1 (Munji *et al*., 2019; Supplementary Figure 1.).

When imaging for PAI-1 expression within the acute phase of stroke (24 hours), this widespread pattern was not yet present. However, we observed a localized pocket of PAI-1 expression, contralateral to the Infarct region (Figure 2b). The only clear connection between the primary somatosensory cortex regions on opposite sides of the brain is the corpus callosum, providing a bilateral neural connection between the two regions. This unique pattern of expression raises

questions. Primarily, how could a protein dependent on pro-fibrotic signalling, ROSs, and pro-inflammatory signalling see an upregulation in expression so far from the site of damage, prior to the widespread upregulation of its respective gene? Furthermore, could this pattern be observed in other EC expressed proteins?

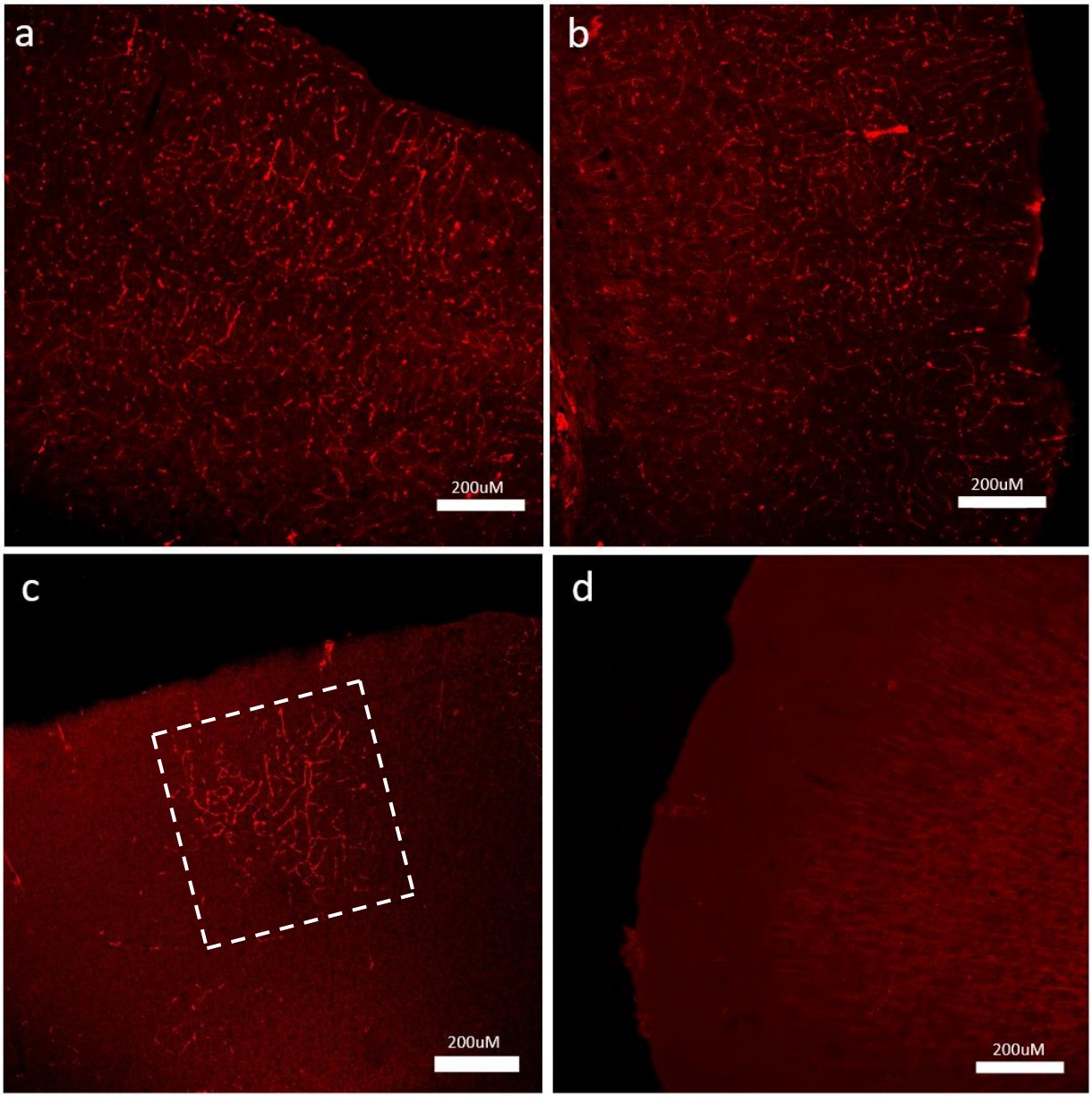

Figure 2. Sample confocal images from pilot study, comparing endothelial cell expression of PAI-1 24 hours and 3 days after photothrombotic stroke. Expression was observed using immunolabelling

technique, with an anti-PAI-1 mouse primary antibody and an anti-mouse Cy5 secondary antibody. **a, b**: Images 3 days following stroke, displaying widespread endothelial cell fluorescence. **a)** Contralateral primary somatosensory cortex. **b)** Contralateral secondary somatosensory cortex. **c, d**: Images 24 hours following stroke, displaying a localized region of endothelial cell expression (highlighted in white box) **c)** Contralateral primary somatosensory cortex. **d)** Contralateral secondary somatosensory cortex. Images captured on 10x objective lens.

ICAM-1 and VCAM-1

Two proteins of interest when determining expression patterns following stroke were Intercellular Adhesion Molecule-1 (ICAM-1/CD54) and Vascular Cell Adhesion Molecule-1 (VCAM-1/CD106). Both ICAM-1 and VCAM-1 are primarily expressed on the membrane of endothelial cells (Hubbard and Rothlein, 2000; Kong *et al.*, 2018). Furthermore, their primary activation of expression is due to the recruitment of pro-inflammatory signalling molecules, such as Tumor necrosis factor alpha (TNFα). Both ICAM-1 and VCAM-1 share a dependence on inflammation in their activation with PAI-1, and with ischemic stroke comes vast inflammation and release of inflammatory cytokines to promote expression of these proteins (Edwards and Bix, 2019). A primary role of these cell adhesion molecules is to bind with surface integrins of rolling leukocytes within the blood vessels and allow for leukocytes to pass through the blood brain barrier and tend to damaged tissue (Langer and Chavakis, 2009).

As previously described, spreading depolarizations can lead to the propagation of cell swelling along grey matter tracts (Hellas and Andrew, 2021). The interaction between cytokine inflammatory signalling, and inflammation due to loss of neuronal membrane potential is not clear. Through investigation of ICAM-1 and VCAM-1 expression patterns following stroke, determining expression of these proteins in regions far from the infarct site could provide insight into potential connections between neural activity and protein expression.

Neurovascular Coupling

The understanding of neural activity and its implications on EC activity is rapidly advancing. The connection between blood flow and neural activity is crucial, as with increased neural activity, the demand for oxygen and glucose increases locally. Within seconds of neural activity, local blood flow increases, producing what is known as the BOLD signal (Hillman, 2015). This signal is the mechanism functional Magnetic Resonance Machines (fMRI) use to determine regions of activity, through localization of deoxyhemoglobin changes (Glover, 2011). Once thought to be a passive cell surrounding blood vessels, ECs have displayed a participation in cell-cell communication through gap junctions (Jackson, 2022) as well as active control of vasodilation and constriction throughout capillary beds (Longden *et al.,* 2021). Other cell types surrounding the environment, such as astrocytes and pericytes, also play a role in the communication between cells and dilation of blood vessels (Bazar, 2016; Hartmann *et al.,* 2022).

With much still unknown regarding the full functionality of ECs, and the potential for neural activity to affect EC processes, could it be possible that neural activity stemming from a SD is responsible for the distant PAI-1 expression we have observed in ECs?

Objectives

The first task was to determine if the application of a neural inhibitor was possible without damaging tissue, as preliminary work from our laboratory indicated that local tissue damage can lead to local expression of PAI-1, which would impact my observations (Supplementary Figure 2). If the passive application of a fluorescein salt produced a localized column of fluorescent

expression, then passive diffusion of a neural inhibitor would be an effective method of silencing activity within the somatosensory cortex.

The next step was to test whether the application of a strong neural inhibitor influenced PAI-1 expression contralateral to the stroke site. If spreading depolarizations are responsible for the expression of PAI-1 contralateral to the stroke site, then local application of a neural inhibitor will decrease PAI-1 expression.

Finally, I wanted to explore if other EC-expressed proteins such as ICAM-1 and VCAM-1 displayed a similar pattern of expression and determine if their expression was potentially dependent on neural activity as well. If spreading depolarizations are responsible for ICAM-1 and VCAM-1 expression, then I will observe a similar contralateral pattern to PAI-1 expression. If so, then the contralateral application of a neural inhibitor will decrease ICAM-1 and VCAM-1 expression.

Methods

Animals

Experiments were performed on C57 male mice, aged 2-4 months. All mice were kept in a 12-hour day/night cycle, with access to laboratory standard food and water *ad libitum*. At least 24 hours prior to experimentation and procedures, cages were kept within the laboratory ventilated rack to minimize environmental stress. All experiments and procedures were conducted according to the guidelines set by the Canadian Council of Animal Care and approved by the University of Victoria Animal Care Committee.

Muscimol/Vehicle Application

Mice were anesthetized using 1.5% isoflurane, while body temperature was kept at 37ºC. The head was fixed in place, and the back of the head was shaved and sterilized. A 1.5cm incision was made on the back of the head, anterior to posterior. 2mm left of bregma, the skull was thinned with a drill, creating a small well (diameter .5mm) above the primary somatosensory cortex forelimb and hindlimb regions (FL/HL). The thinned skull was poked with a 29G syringe tip, puncturing the skull. Solution was then pipetted onto the well and allowed to diffuse through the hole over 5-7 minutes.

To initially determine the spread of solution following diffusion, 1µL of 2% Fluorescein Salt was pipetted (1% Fluorescein Salt in Artificial Cerebral-Spinal Fluid (ACSF)). Tissue was collected 30 minutes after application to be imaged.

To inhibit local neural activity, a Muscimol solution was applied. This solution contained one-part Muscimol at 20µg/µL, one-part 2% 2MDa FITC in ACSF, and one-part ACSF. This produces an application of 58mM of Muscimol. For control applications, vehicle solution contained one-part 2% 2MDa FITC in ACSF and two parts ACSF. Tissue was collected 24 hours following application.

Photothrombotic Stroke

Photothrombotic stroke was based off the model stated by Watts *et at*. (2015). Mice were anesthetized using 1.5% isoflurane and body temperature maintained at 37ºC. The head was fixed in place, and the back of the head was shaved and sterilized. A 1.5cm incision was made on the back of the head. 2mm right of Bregma, above the primary somatosensory cortex FL/HL, the

skull was thinned with a drill. A Rose Bengal dye (10µg/mL in ACSF) was injected into the peritoneum (IP injection). Total volume of injection was determined by body weight per mouse (100mg/kg). A 532nm laser was applied to the thinned region of the skull for 4-7 minutes. In conditions where a photothrombotic stroke was performed and solution was applied to the contralateral primary somatosensory cortex, the stroke was performed first. In conditions where stroke was not performed, drilling and application of 532nm laser were completed, however no Rose Bengal dye was injected.

Perfusion, Extraction, and Slicing of Tissues

To determine Fluorescein Salt diffusion, 30 minutes following solution application brains were extracted from deeply anesthetized mice and fixed in 4% paraformaldehyde (PFA) in 0.1M phosphate buffered saline (PBS) overnight at 4ºC. Brains were sliced coronally 200µm thick using a Leica VT1200 vibrating microtome. Tissue 1mm anterior or posterior of bregma were imaged for analysis.

For immunolabelling experimentation, 24 hours following a photothrombotic stroke or sham, brains were extracted from deeply anesthetized mice. The right atrium of the heart was cut while still beating, and the left ventricle of the heart was slowly injected with 6mL PBS, followed by 6mL of 4% PFA to perfuse and fix tissue. Tissue was stored overnight in 4% PFA and then transferred to 30% sucrose solution in 01.M PBS + 0.02% Sodium Azide for storage. Brains were sliced coronally 50µm thick using a freezing microtome. Tissue 1mm anterior or posterior of bregma were used for analysis.

Immunolabelling of PAI-1, ICAM-1, and VCAM-1

Following sectioning of brain tissue, slices were stored in PBS + 0,02% Sodium Azide. To perform immunolabelling for PAI-1, VCAM, and ICAM, staining protocols were followed (see appendices 1 and 2). The antigen retrieval step was only performed for PAI-1 immunolabelling. For control conditions, application of the primary antibody was skipped, producing a no primary condition. Following labelling process, tissue was mounted on a Gelatin-coated slides and cover slipped with Fluoromount G. the primary antibodies used were: Biolegend Rat anti-mouse CD54 (ICAM-1) Antibody, Millipore Sigma Rat anti-Mouse CD106 (VCAM-1), and Invitrogen PAI-1 Monoclonal Antibody. The secondary antibodies used were: Goat anti-Mouse IgG (H+L) Cross-Adsorbed Secondary Antibody Cyanine5, and Goat anti-Rat IgG (H+L) Cross-Adsorbed Secondary Antibody Cyanine5.

Fluorescence Imaging and Analysis

For Fluorescein Salt analysis, images were taken on an Olympus BX50WI Microscope. All analysis was performed in ImageJ. Spread of fluorescence was determined using the Ostu threshold method. Measurements of fluorescence were taken and compared to stereotaxic coordinates as stated by The Allen Institute for Brain Science (2004) (Figure 3d).

For immunolabelling analysis, confocal Z-stacks were taken on an Olympus confocal microscope with a step size of 2µm. Images were taken at 1024x1024 pixel resolution, with a size of 1.6103 pixels/micron, through a 20x objective lens (NA 0.75). Analysis of these images followed the procedure outlined in appendix 3, performed on Prism 10.2.1 software. Analysis provided a percentage of each image expressing fluorescence above threshold. Comparisons between two conditions (Figure 5d, 6h) were compared using either a paired or unpaired t-test,

dependent on whether values originated from the same brain samples. Comparisons between three conditions were compared using a One Way ANOVA and Fisher's LSD post hoc test (Figure 6d). Comparisons between more than three conditions were made using a One Way ANOVA and Tukey's post hoc test (Figure 6k,l).

IgG Fragment Antibody Blocking

In experiments where antibody blocking was attempted, an IgG Fragment antibody (Millipore Sigma Anti-Mouse IgG (Fab specific) antibody produced in goat) was applied to tissue prior to immunolabelling following the prepared protocol (see appendix 4). To produce a no primary condition, the primary antibody step was skipped.

Results

Fluorescein Salt Diffusion

My first experiment was to determine the effectiveness of drug application through passive diffusion (Figure 3a, Muscimol/Vehicle application in methods). The threshold image displayed that the spread of fluorescence produced a localized column (Figure 3b). The column resided 1.06mm from the midline of the brain and extended as far as 2.65mm from the midline (Figure 3c). The max width of the fluorescence reached 1.7mm across, and a max depth of 1.56mm. The total area covered was 2.07mm^2 at bregma. These measurements of expression closely resemble the stereotaxic measurements of the Forelimb and Hindlimb regions of the primary somatosensory cortex (Figure 3d). Fluorescence spread to slices both rostral and caudal of bregma approximately 1mm, consistent with an area of diffusion of ~2mm^2. Fluorescein Salt

used in this experiment to visualize spread of diffusion has a molecular weight of 412.3 Da, a greater weight than muscimol (114.1 Da), indicating that muscimol should effectively diffuse into the contralateral region of the brain (National Center for Biotechnology Information, 2024).

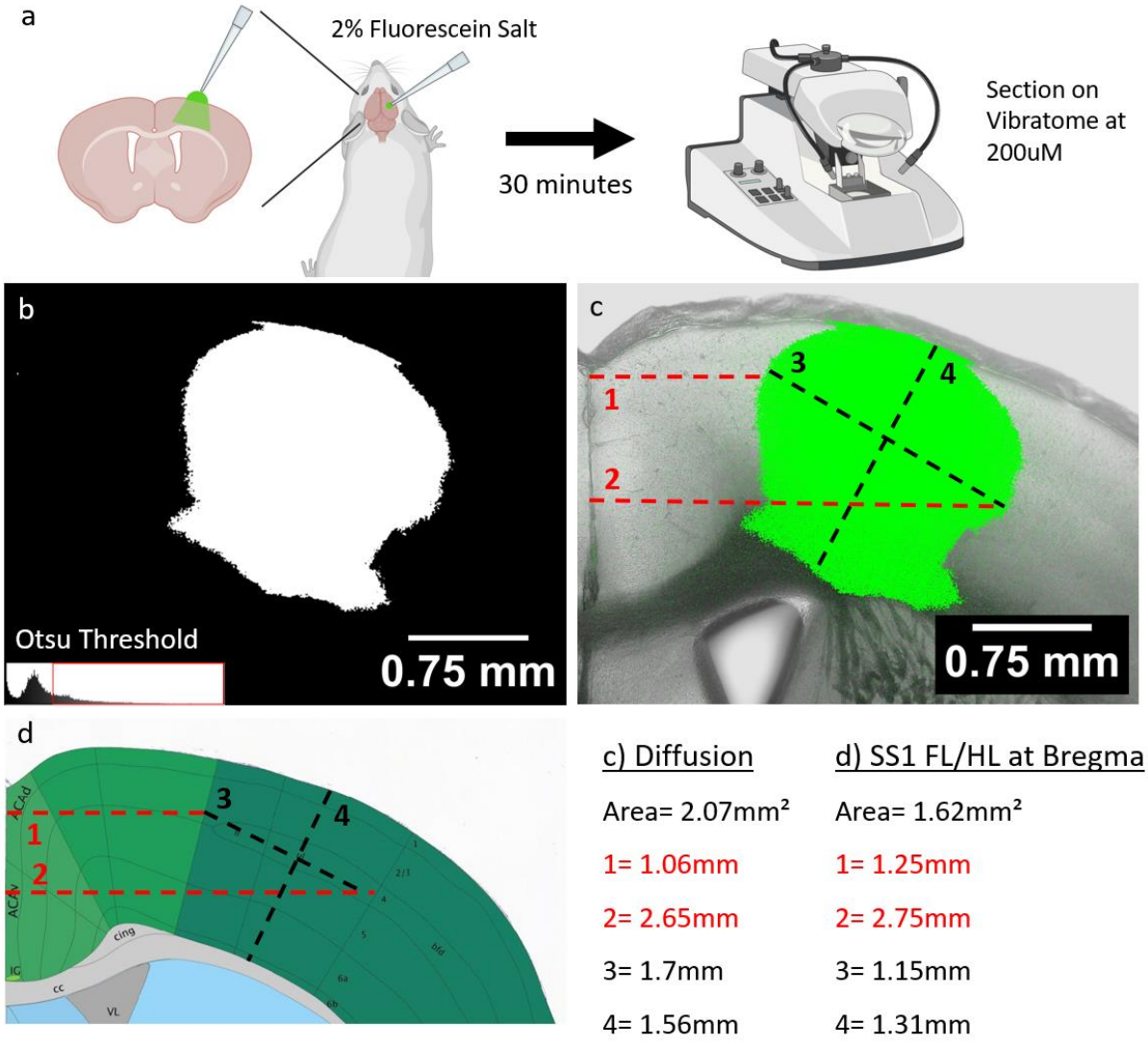

Figure 3. Application of Fluorescein Salt to determine effectiveness of diffusion method. **a)** Visual representation of diffusion method. 30 Minutes following diffusion, brain was perfused and extracted. Brain was sectioned coronally at 200µm thick using a Leica VT1200 vibrating microtome. **b)** Threshold image of fluorescence from Fluorescein Salt. Otsu threshold was used to determine threshold region. **c, d)** Comparison between diffusion region of the fluorescence threshold image (**c**) and stereotaxic coordinates of the primary somatosensory Forelimb and Hindlimb region (SS1 FL/HL) (**d**). Area, nearest

distance from midline (1, red line), furthest distance from midline (2, red line), max width (3, black line), and max depth (4, black line) were compared.

PAI-1 Expression Following Stroke and Muscimol Application

The next experiment was to determine if the application of muscimol would decrease contralateral PAI-1 expression (Figure 4a). Following immunolabelling expression appeared widespread across the brain, for each condition, including those subjected to a sham stroke. This finding contradicts the initial pattern observed in Figure 2. Following a no primary test, where the primary antibody was not applied to the tissue, fluorescent labelling persisted. Furthermore, I observed a pattern of labelling that appeared striped along the blood vessels (Figure 4b). This spotted expression made up the vast majority of expression above threshold (Figure 4c).

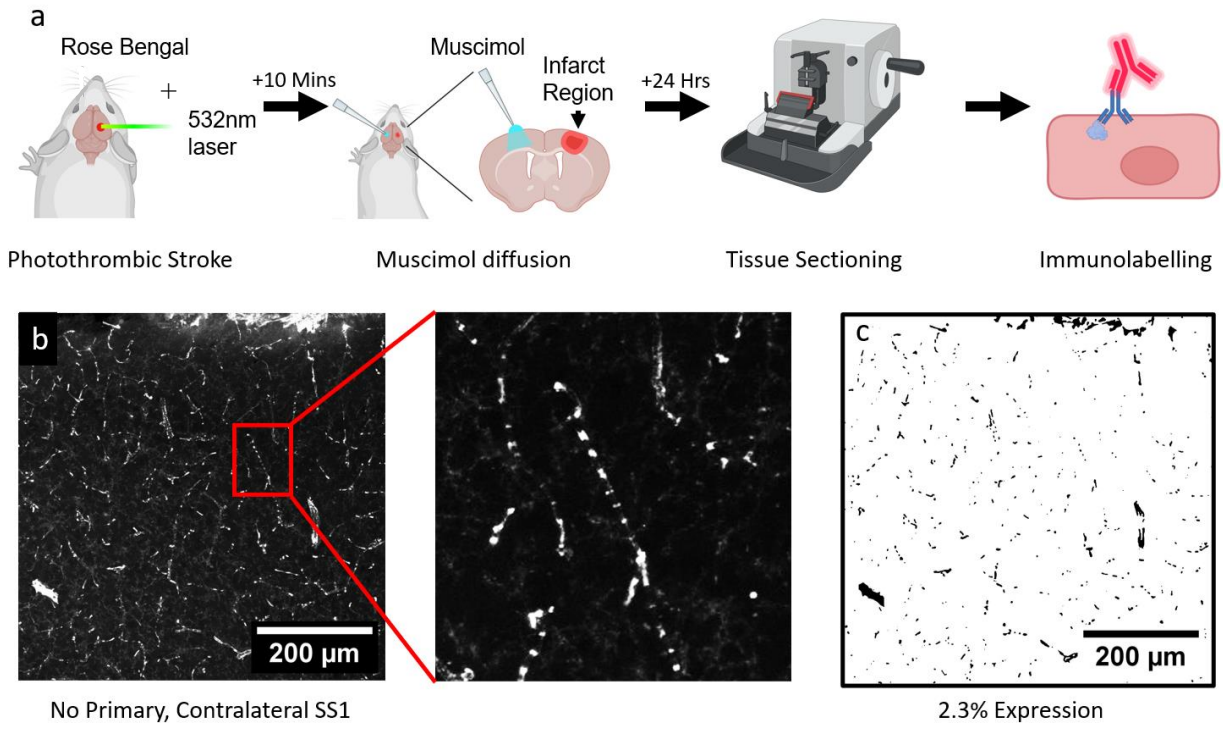

Figure 4. Expression of PAI-1 following photothrombotic stroke and muscimol application. **a)** Experimental setup, displaying photothrombotic stroke model, muscimol diffusion, tissue sectioning, and

immunolabelling. **b)** Image in contralateral primary somatosensory cortex, under 'no primary' condition where no secondary antibody was applied. Zoomed image displays striped expression of blood vessel. **c)** Threshold of image b, displaying an expression percentage of 2.3%.

IgG Fragment Antibody Blocking

As the results yielded from the no primary control in Figure 4 were not as expected, I attempted to address the cause of the spotted expression. I hypothesized that the secondary anti mouse antibodies were recognizing and binding to endogenous IgG antibodies within the blood plasma instead of the desired PAI-1 within EC's. To address this, I applied a fragment antibody to recognize the endogenous IgG, block the signal, and theoretically decrease the expression of fluorescence in the no primary control (Figure 5a, see methods section on IgG fragment antibody blocking). Contralateral regions were compared within two of the same brains previously measured to determine if a decrease in fluorescence would occur. As observed in Figure 5b and c, the spotted expression of fluorescence did not appear to change, and statistical analysis of images confirmed that fluorescence did not drop (Figure 5d). This suggests that application of the fragment antibody was not sufficient to decrease spotted fluorescence in a no primary condition.

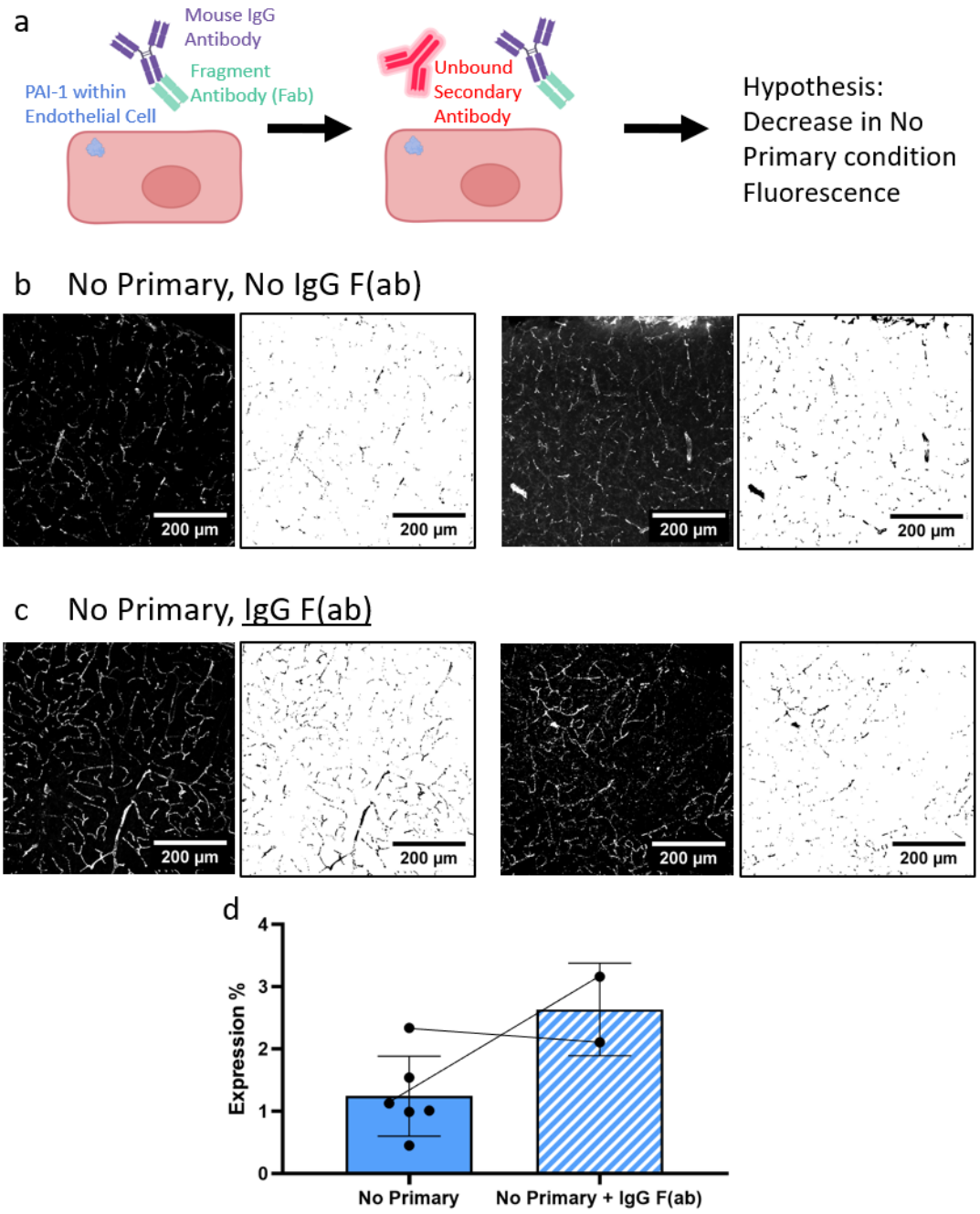

Figure 5. Application of fragment antibody blocking to block IgG antibody recognition. **a)** Hypothesized effect of fragment antibody application, where no primary condition observes a decrease in fluorescence expression %. **b)** Images of no primary condition prior to application of fragment antibody (n=6). **c)** Images from same two samples with fragment antibody applied prior to secondary antibody (n=2). **d)** Quantification of expression % from threshold images. No significant change was observed between no primary and no primary + fragment antibody conditions (Paired t test, P = .5718).

ICAM-1 and VCAM-1 Expression Following Stroke and Muscimol Application

For my final experiment, I wanted to determine if a similar pattern of expression to Figure 2 could be replicated with ICAM-1 and VCAM-1 proteins. First, a pilot test was performed to see if the primary antibodies for ICAM-1 and VCAM-1 could provide an accurate fluorescent representation of proteins in comparison to a no primary control (Figure 6a-d). While the primary VCAM-1 antibody did not provide robust fluorescence (0.502%, 5 images), ICAM-1 was clearly expressed at a significantly greater level at peri infarct regions (3.507%, 5 images) than the no primary condition (0.617%, 5 images). Crucially, the no primary condition (Figure 6a) did not display a similar spotted pattern to that in Figure 4b, and threshold percentages were low. Next, I wanted to determine if the expression of ICAM-1 fluorescence was dependent on the applied stroke model. (Figure 6e-h). The sham stroke models did not display any notable fluorescence (0.8201%, n=4) , and images taken both laterally and medially of the stroke site yielded a significantly higher expression % (3.507%, n=5).

The next task was to determine if contralateral to the stroke site a localized expression formed, and whether application of muscimol would influence contralateral expression (Figure 6i-k). No significant differences were measured between sham (0.714%, n=2) and stroke (1.793%, n=3) conditions in contralateral expression, however visibly there was a slightly greater presence of vessel labelling, as indicated by the yellow arrows in figure 6j. The application of muscimol had no evident effect on ICAM-1 expression in conditions with (1.603%, n=2) and without stroke (1.172%, n=2). Following the general expression pattern of ICAM-1 (Figure 6l) in brains with stroke and no muscimol, greater expression % appeared to be correlated with proximity to the stroke site (n=3).

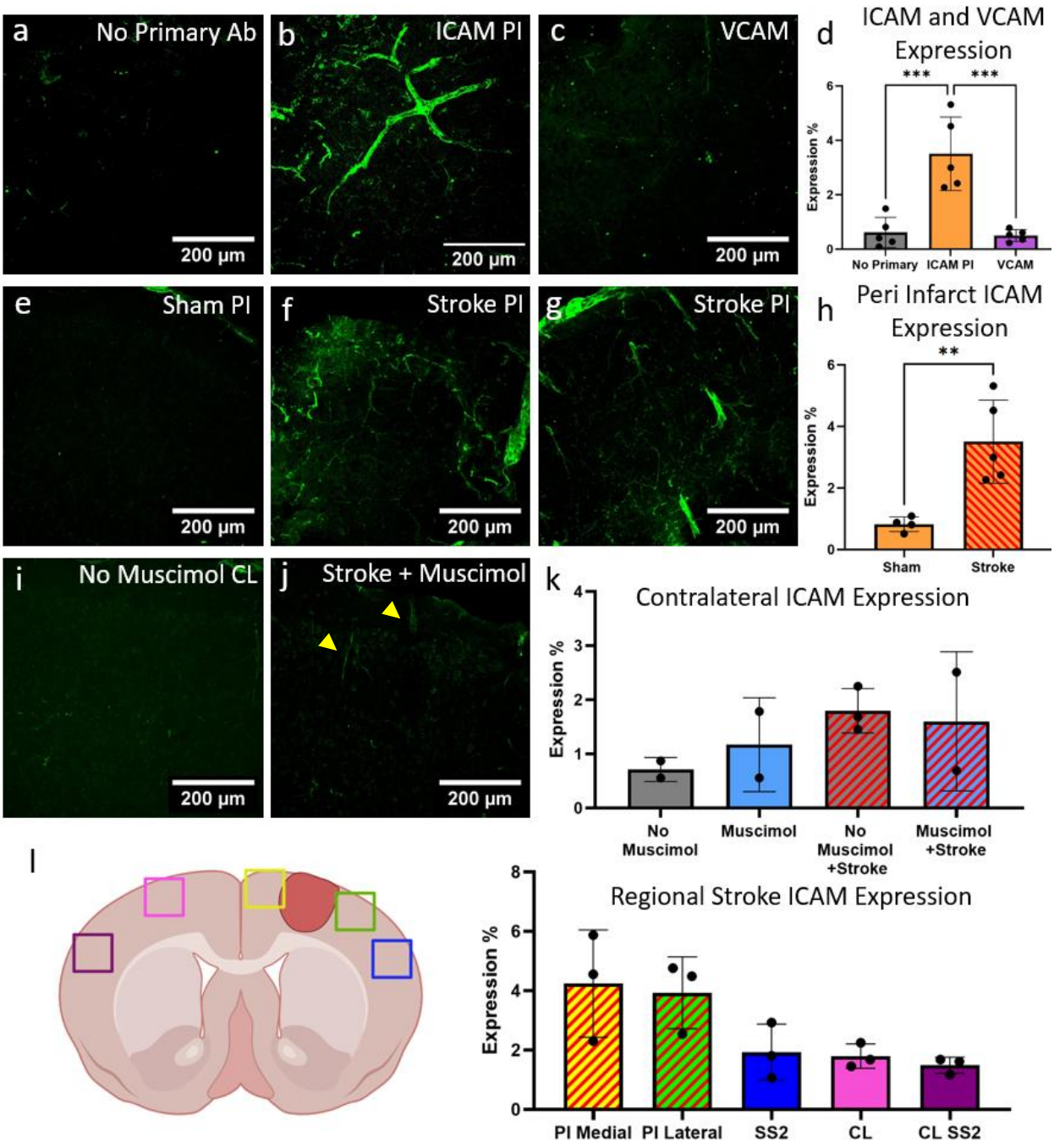

Figure 6. Expression of ICAM and VCAM following stroke. **a,b,c,d)** Comparison of ICAM and VCAM to no primary condition. **a** displays expression at the peri infarct under no primary conditions, **b** at the peri infarct site with the ICAM primary antibody, and **c** at the peri infarct site with the VCAM primary antibody. **d** displays the results of each condition (One way ANOVA with Fisher's LSD post hoc test). **e,f,g,h**) Comparison of ICAM expression at the peri infarct region of brains under sham and stroke conditions. **e** displays ICAM expression in a sham peri Infarct region. **f,g** display ICAM expression in a

stroke peri Infarct region. **h** summarizes results (Unpaired t test). **i,j,k**) Comparison of ICAM expression following muscimol application at contralateral primary somatosensory cortex. **i** displays ICAM expression without stroke or muscimol applied. **j** displays with stroke and muscimol applied. **k** summarizes findings (One way ANOVA with Tukey's HSD post hoc test). **l**) comparison of ICAM expression by region following stroke, with no muscimol application (One way ANOVA with Tukey's HSD post hoc test). ** = $P < .005$, *** = $P < .0005$.

Discussion

In summary, my first hypothesis predicted a passive diffusion method would be an effective method of drug application while mitigating tissue damage. The application of Fluorescein salt effectively produced a localized column of fluorescent expression in the primary somatosensory cortex, without inserting a needle into the brain tissue. My second hypothesis theorized the contralateral application of muscimol following a stroke model would decrease the localized expression pattern of PAI-1. The immunolabelling process for PAI-1 was not a successful assay, as a spotted pattern of vessels within the no primary control led to an increased basal level of expression. This led to a new hypothesis, that the application of a fragment antibody to block IgG endogenous antibody binding would decrease fluorescent expression in a no primary control. This hypothesis was not supported, as spotted expression persisted, and expression levels did not decrease. Finally, I hypothesized that ICAM-1 and VCAM-1 would display a dependence on stroke for protein expression, and that a similar contralateral pattern of expression would occur to that observed with PAI-1. While ICAM-1 did display a dependence on stroke damage for expression, VCAM-1 did not. Furthermore, ICAM-1 did not produce a localized contralateral region of expression, but rather a dependency on proximity to the stroke site.

Fluorescein Salt and Muscimol Application

The reasoning of producing a new method for drug application stems from initial pilot studies performed in our laboratory indicating that local tissue damage can induce PAI-1 expression (See supplementary figure 2). As measurements of PAI-1 would have been affected, it was important to test this new method. To reduce bias in the analysis of fluorescence, the Otsu threshold method was used, which provides a strong threshold analysis for bimodal distributions, such as the fluorescent images taken in this experiment (Jianzhuang *et al*., 1991). When compared with stereotaxic coordinates, the localized column appears to effectively cover the forelimb and hindlimb region of the primary somatosensory cortex. While stereotaxic coordinates are a rough mapping of brain activity, they still provide a strong basis for functional regions when operating on the scale at which I did, not reaching down to individual neuronal networks but instead large general regions of the brain.

The application of muscimol through this method depends on certain presumptions. First, while muscimol is a smaller molecule (114.1 Da) than the Fluorescein salt (412.3 Da) used for this fluorescent tracking and should be able to diffuse through brain tissue at a similar rate, there is no guarantee that the diffusion would follow an identical pattern. For future research, a muscimol molecule bound to a small fluorophore conjugate, such as BODIPY™ TMR-X Conjugate (Invitrogen, Product #M23400), would allow for confirmation of where muscimol spreads, cancelling out the need for a proxy marker (Allen *et al*., 2008). Another assumption of this experiment is that muscimol would effectively inhibit the activity of a spreading depolarization. While previous work from the laboratory has provided both behavioural and intrinsic optical imaging results indicating that muscimol does inhibit neural activity when applied at a similar concentration (Reeson *et al.*, 2022; Sweetnam *et al.,* 2012), the activity in those conditions were

specific and action potential dependent. Spreading depolarizations, however, produce a slow rise in resting membrane potential due to ATPase pump failure (Andrew *et al.*, 2022). While muscimol has been proven to inhibit standard neural activity, there is no indication as to whether spreading depolarizations are effectively inhibited by a GABA-A receptor agonist (See Table 1 of Andrew *et al*., 2022). While it is possible that the silencing of neural activity would be sufficient, the application of a tried and tested spreading depolarization antagonist could be an option in future research, along with a greater understanding of the primary mechanisms driving spreading depolarizations.

PAI-1 Expression and Endogenous Antibody Blocking

The second experiment was initially devised to determine if the pattern of PAI-1 expression could be altered with the application of muscimol to the contralateral region. This experiment was not an effective assay, as it failed to pass control experiments. When the anti- PAI-1 antibody step was skipped the secondary anti-mouse antibody still produced fluorescence, in a spotted pattern across blood vessels. The best estimation as to why this occurred is due to the quality of tissue perfusion. When working with an anti-mouse secondary antibody to image for endothelial cell expression, complete removal of blood plasma is crucial. This is due to the presence of different antibodies within the blood plasma which the secondary antibody may be recognizing. The five categories of immunoglobulins found within mammals are IgM, IgD, IgG, IgA, and IgE (Alberts *et al*., 2002). The spotted pattern of fluorescence within the no primary controls likely displays the blood plasma between the gaps of red blood cells passing through the capillary vessels, where the endogenous antibodies are present.

The third experiment was an attempt to limit this endogenous antibody expression. As IgG is the most prominent immunoglobulin form in blood plasma, I attempted to decrease the likelihood that the secondary antibody would bind to endogenous IgG's. This was done through the application of a fragment antibody (the small binding portion of an antibody) to bind to the excess IgG, theoretically decreasing the fluorescence expression under no primary conditions. As observed in Figure 5, this did not effectively decrease the expression. This likely was not an effective approach for two reasons. First, the fragment antibody applied may not be sufficiently blocking all the IgG present within the plasma. Recommendations from Proteintech (2024) suggests a concentration of 0.1 mg/mL, significantly higher than the concentration used here, for effective blocking. However, even at a lower concentration, a partial decrease in fluorescence would have been expected if this was the only factor at play. A second possibility is that other forms of immunoglobulins were also present within the plasma, which remained unaffected by the fragment antibody. Other forms of immunoglobulin spring to action following the acute phase of stroke from the adaptive immune system (Iadecola, 2020), which may be contributing to the persistent fluorescence.

For future research, a more assured perfusion to remove blood from the vessels would ensure that any remaining plasma is removed from the tissue. This could include the addition of an anticoagulant to the PBS injected in the extraction process, such as heparin, to avoid aid in the removal of the plasma.

These findings did not reaffirm, nor disprove the initial findings of PAI-1 expression (Figure 2), so the possibility of expression being dependent on neural activity remains. It is not clear whether the contralateral expression is an artifact of procoagulant responses to the evolutionarily relevant hemorrhagic stroke, or an active mechanism of neuroprotection for neurons spanning

across the corpus callosum from the infarct region (Cho *et al.*, 2012; Docagne *et al*., 2002; Soeda *et al*., 2008).

Potential pathways that promote PAI-1 expression, described by Rahmen *et al*. (2020), include pro-fibrotic, pro-inflammatory, and hormonal signalling. Hormonal signalling appears the least likely of these possibilities in producing a localized expression contralateral to the stroke site, as hormones are released into the blood stream indirectly, and depend on specificity of receptors. The likelihood or purpose of a receptor localization to hormones in the primary somatosensory region is low. Inflammatory signalling may be responsible for PAI-1 expression contralateral to the stroke site, as cell swelling can incur from the spread of a spreading depolarization. However, ICAM-1 plays a critical role in inflammatory signalling and does not appear to express a contralateral pattern in the same way, but rather a proximity specific expression from the stroke site.

It is worth considering what aspects of the SD could cause implications on the contralateral side of the brain. If the SD propagates along the grey matter tracts of neurons, then contralaterally an increase in $[K^+]o$ and $[Na^+]i$ would be observed due to a loss of ATPase pump activity . As the local tissue is still effectively perfused by blood flow, ATP and oxygen concentrations shouldn't be largely affected. An increase in $[K^+]o$ plays a key role in neurovascular coupling, as one of the major promoters of vascular relaxation (Jackson, 2022). Preliminary research has shown that the tPA/PAI-1 axis may also have implications for vascular relaxation/ dilation (Nassar *et al.,* 2011; Furon *et al.,* 2023). This implies the possibility that extended exposure of $[K^+]o$ could lead to multiple effects of vascular relaxation, possibly through the tPA/PAI-1 axis in addition to the more well-known K^+ inward rectifier channels. Alternatively, the vasodilation following $[K^+]o$ increase could be what promotes the PAI-1 expression through mechanosensing channels on the

EC. Mechanosensation of blood flow by ECs through various mechanosensory channels and ion channels could provide another alternative expression of PAI-1 (Lim and Haraz, 2024).

ICAM-1 Expression Following Stroke

In the final experiment, I hypothesized that ICAM-1 and VCAM-1 would display an increase in expression following stroke, mimicking the contralateral pattern seen in PAI-1 expression. While VCAM-1 did not appear to change greatly following stroke, ICAM-1 did display a significant increase in expression. However, it did not appear to express contralaterally, but instead following a proximity pattern. Regions close to the stroke site observed a greater expression, and distal regions experienced less expression. A notable observation of ICAM-1 expression is that it appeared less localized in the small capillary branches (such as PAI-1 in Figure 2), but instead in ECs surrounding larger blood vessels. This is consistent with ICAM-1's function, binding to Mac-1, an integrin on rolling leukocytes, and directing them to regions of tissue inflammation (Langer and Chavakis, 2009). This process of leukocyte rolling occurs largely in post capillary venules, not capillaries, explaining the larger blood vessel expression. As for the proximity expression from the stroke site, this reaffirms the idea that inflammation is greater at the infarct and peri infarct region, and inflammatory signals may not propagate with neural activity as a SD would. Though contralateral tissue may see the effects of SD, tissue far from the infarct region usually remains healthy and perfused, implying less inflammatory signalling within the region.

Future considerations

Research regarding the tPA/PAI-1 axis has grown since the application of tPA therapy following ischemic stroke (The National Institute of Neurological Disorders and Stroke rt-PA Stroke Study Group, 1995), however the development of therapeutic advancements often precedes true understanding of underlying mechanism. With the understanding of neurovascular coupling and spreading depolarizations rapidly advancing, understanding the interplay between these mechanisms throughout stroke development is crucial. Furthermore, no clear explanation currently exists on why such a pattern of expression would occur. Particularly in PAI-1, a procoagulant expressed within endothelial cells, when the only clear connection between the contralateral primary somatosensory cortex and the infarct region following stroke is the neural bilateral connections of the corpus callosum. Investigating if any other possible factors promoting the expression of PAI-1 (in addition to those described by Kahman *et al.,* 2020) would be a clear first step, along with confirming the expression observed through mature RNA analysis of the contralateral brain tissue (similar to that of supplementary figure 2).

Understanding this expression could provide further insight into how the brain responds following stroke and how potential treatment could be applied in a less invasive fashion. If certain responses to stroke have bilateral expression, then the contralateral application of therapeutic drugs may provide a potential benefit.

While the results of ICAM-1 imaging largely support previous findings and clarify the likely expression of inflammatory factors following stroke, VCAM-1 was not conclusive. While it appeared that very vague vessels were labelled following VCAM-1 staining, it was far from surpassing the expression of the no primary condition. Whether VCAM-1 immunolabelling was not an effective assay, or ICAM-1 expression was considerably higher is unclear. Developing an

effective VCAM-1 immunolabelling protocol under conditions where VCAM-1 expression would be guaranteed to express would be a suitable first step for future research. Clear expression of VCAM-1 could provide further insight into the role of leukocyte rolling within venules following stroke.

In summary, my research displayed an effective method of drug application while minimizing tissue damage that can add value to a wide range of pharmacological research in mice models. Furthermore, I provide commentary on the role of the tPA/PAI-1 axis following stroke, highlighting that further investigation is required in the relationship between neurovascular coupling, spreading depolarizations, and PAI-1 expression. Lastly, my research reaffirms the inflammatory response and role of ICAM-1 following stroke.

References

Alberts, B., Johnson, A., Lewis, J., Raff, M., Roberts, K., & Walter, P. (2002) Molecular Biology of the Cell. 4th edition. https://www.ncbi.nlm.nih.gov/books/NBK26884/

Allen, T. A., Narayanan, N. S., Kholodar-Smith, D. B., Zhao, Y., Laubach, M., & Brown, T. H. (2008). Imaging the spread of reversible brain inactivations using fluorescent muscimol. *Journal of Neuroscience Methods*, *171*(1), 30–38. https://doi.org/10.1016/j.jneumeth.2008.01.033

Allen Institute for Brain Science (2004). *Mouse Brain Atlas.* https://atlas.brain-map.org/atlas?atlas=1#atlas=1&plate=100960309&structure=549&x=5279.99951171875&y=3743.999994277954&zoom=-4&resolution=16.75&z=5

Andrew, R. D., Farkas, E., Hartings, J. A., Brennan, K. C., Herreras, O., Müller, M., Kirov, Sergei. A., Ayata, C., Ollen-Bittle, N., Reiffurth, C., Revah, O., Robertson, R. M., Dawson-Scully, K. D., Ullah, G., & Dreier, J. P. (2022). Questioning Glutamate Excitotoxicity in Acute Brain Damage: The Importance of Spreading Depolarization. *Neurocritical Care*, *37*(S1), 11–30. https://doi.org/10.1007/s12028-021-01429-4

Barthels, D., & Das, H. (2020). Current advances in ischemic stroke research and therapies. *Biochimica et Biophysica Acta (BBA) - Molecular Basis of Disease*, *1866*(4), 165260. https://doi.org/10.1016/j.bbadis.2018.09.012

Bazargani, N., & Attwell, D. (2016). Astrocyte calcium signaling: The third wave. *Nature Neuroscience*, *19*(2), 182–189. https://doi.org/10.1038/nn.4201

Callegari, K., Dash, S., Uchida, H., Shingai, Y., Liu, C., Khodarkovskaya, A., Lee, Y., Ito, A., Lopez, A., Zhang, T., Xiang, J., Kluk, M. J., & Sanchez, T. (2023). Molecular profiling of the stroke-induced alterations in the cerebral microvasculature reveals promising therapeutic candidates.

Proceedings of the National Academy of Sciences, *120*(16), e2205786120. https://doi.org/10.1073/pnas.2205786120

Cho, H., Joo, Y., Kim, S., Woo, R.-S., Lee, S. H., & Kim, H.-S. (2012). Plasminogen Activator Inhibitor-1 Promotes Synaptogenesis and Protects Against Aβ $_{1-42}$ -Induced Neurotoxicity in Primary Cultured Hippocampal Neurons. *International Journal of Neuroscience*, *123*(1), 42–49. https://doi.org/10.3109/00207454.2012.724127

Czéh, G., Aitken, P. G., & Somjen, G. G. (1993). Membrane currents in CA1 pyramidal cells during spreading depression (SD) and SD-like hypoxic depolarization. *Brain Research*, *632*(1–2), 195–208. https://doi.org/10.1016/0006-8993(93)91154-K

Desai, J. A., & Smith, E. E. (2013). Prenotification and Other Factors Involved in Rapid tPA Administration. *Current Atherosclerosis Reports*, *15*(7), 337. https://doi.org/10.1007/s11883-013-0337-5

Dreier, J. P., Fabricius, M., Ayata, C., Sakowitz, O. W., William Shuttleworth, C., Dohmen, C., Graf, R., Vajkoczy, P., Helbok, R., Suzuki, M., Schiefecker, A. J., Major, S., Winkler, M. K., Kang, E.-J., Milakara, D., Oliveira-Ferreira, A. I., Reiffurth, C., Revankar, G. S., Sugimoto, K., Hartings, J. A. (2017). Recording, analysis, and interpretation of spreading depolarizations in neurointensive care: Review and recommendations of the COSBID research group. *Journal of Cerebral Blood Flow & Metabolism*, *37*(5), 1595–1625. https://doi.org/10.1177/0271678X16654496

Edwards, D. N., & Bix, G. J. (2019). The Inflammatory Response After Ischemic Stroke: Targeting β2 and β1 Integrins. *Frontiers in Neuroscience*, *13*, 540. https://doi.org/10.3389/fnins.2019.00540

Furon, J., Yetim, M., Pouettre, E., Martinez De Lizarrondo, S., Maubert, E., Hommet, Y., Lebouvier, L., Zheng, Z., Ali, C., & Vivien, D. (2023). Blood tissue Plasminogen Activator (tPA) of liver origin contributes to neurovascular coupling involving brain endothelial N-Methyl-D-Aspartate (NMDA) receptors. *Fluids and Barriers of the CNS*, *20*(1), 11. https://doi.org/10.1186/s12987-023-00411-w

George, M. G. (2020). Risk Factors for Ischemic Stroke in Younger Adults: A Focused Update. *Stroke*, *51*(3), 729–735. https://doi.org/10.1161/STROKEAHA.119.024156

Glover, G. H. (2011). Overview of Functional Magnetic Resonance Imaging. *Neurosurgery Clinics of North America*, *22*(2), 133–139. https://doi.org/10.1016/j.nec.2010.11.001

Hartmann, D. A., Coelho-Santos, V., & Shih, A. Y. (2022). Pericyte Control of Blood Flow Across Microvascular Zones in the Central Nervous System. *Annual Review of Physiology*, *84*(1), 331–354. https://doi.org/10.1146/annurev-physiol-061121-040127

Hellas, J. A., & Andrew, R. D. (2021). Neuronal Swelling: A Non-osmotic Consequence of Spreading Depolarization. *Neurocritical Care*, *35*(S2), 112–134. https://doi.org/10.1007/s12028-021-01326-w

Hillman, E. M. C. (2014). Coupling Mechanism and Significance of the BOLD Signal: A Status Report. *Annual Review of Neuroscience*, *37*(1), 161–181. https://doi.org/10.1146/annurev-neuro-071013-014111

Holodinsky, J. K., Lindsay, P., Yu, A. Y. X., Ganesh, A., Joundi, R. A., & Hill, M. D. (2022). Estimating the Number of Hospital or Emergency Department Presentations for Stroke in Canada. *Canadian Journal of Neurological Sciences / Journal Canadien Des Sciences Neurologiques*, 1–6. https://doi.org/10.1017/cjn.2022.338

Hong, J. M., Kim, D. S., & Kim, M. (2021). Hemorrhagic Transformation After Ischemic Stroke: Mechanisms and Management. *Frontiers in Neurology*, *12*, 703258. https://doi.org/10.3389/fneur.2021.703258

Hubbard, A. K., & Rothlein, R. (2000). Intercellular adhesion molecule-1 (ICAM-1) expression and cell signaling cascades. *Free Radical Biology and Medicine*, *28*(9), 1379–1386. https://doi.org/10.1016/S0891-5849(00)00223-9

Iadecola, C., Buckwalter, M. S., & Anrather, J. (2020). Immune responses to stroke: Mechanisms, modulation, and therapeutic potential. *Journal of Clinical Investigation*, *130*(6), 2777–2788. https://doi.org/10.1172/JCI135530

Jackson, W. F. (2022). Endothelial Ion Channels and Cell-Cell Communication in the Microcirculation. *Frontiers in Physiology*, *13*, 805149. https://doi.org/10.3389/fphys.2022.805149

Jeon, H., Kim, J.-H., Kim, J.-H., Lee, W.-H., Lee, M.-S., & Suk, K. (2012). Plasminogen activator inhibitor type 1 regulates microglial motility and phagocytic activity. *Journal of Neuroinflammation*, *9*(1), 149. https://doi.org/10.1186/1742-2094-9-149

Kong, D.-H., Kim, Y., Kim, M., Jang, J., & Lee, S. (2018). Emerging Roles of Vascular Cell Adhesion Molecule-1 (VCAM-1) in Immunological Disorders and Cancer. *International Journal of Molecular Sciences*, *19*(4), 1057. https://doi.org/10.3390/ijms19041057

Langer, H. F., & Chavakis, T. (2009). Leukocyte – endothelial interactions in inflammation. *Journal of Cellular and Molecular Medicine*, *13*(7), 1211–1220. https://doi.org/10.1111/j.1582-4934.2009.00811.x

Leao, A. A. P. (1947). Further observations on the spreading depression of activity in the cerebral cortex. *Journal of Neurophysiology*, *10*(6), 409–414. https://doi.org/10.1152/jn.1947.10.6.409

Lim, X. R., & Harraz, O. F. (2024). Mechanosensing by Vascular Endothelium. *Annual Review of Physiology*, *86*(1), 71–97. https://doi.org/10.1146/annurev-physiol-042022-030946

Liu Jianzhuang, Li Wenqing, & Tian Yupeng. (1991). Automatic thresholding of gray-level pictures using two-dimension Otsu method. *1991 International Conference on Circuits and Systems*, 325–327. https://doi.org/10.1109/CICCAS.1991.184351

Longden, T. A., Mughal, A., Hennig, G. W., Harraz, O. F., Shui, B., Lee, F. K., Lee, J. C., Reining, S., Kotlikoff, M. I., König, G. M., Kostenis, E., Hill-Eubanks, D., & Nelson, M. T. (2021). Local IP_3 receptor–mediated Ca^{2+} signals compound to direct blood flow in brain capillaries. *Science Advances*, *7*(30), eabh0101. https://doi.org/10.1126/sciadv.abh0101

Munji, R. N., Soung, A. L., Weiner, G. A., Sohet, F., Semple, B. D., Trivedi, A., Gimlin, K., Kotoda, M., Korai, M., Aydin, S., Batugal, A., Cabangcala, A. C., Schupp, P. G., Oldham, M. C., Hashimoto, T., Noble-Haeusslein, L. J., & Daneman, R. (2019). Profiling the mouse brain endothelial transcriptome in health and disease models reveals a core blood–brain barrier dysfunction module. *Nature Neuroscience*, *22*(11), 1892–1902. https://doi.org/10.1038/s41593-019-0497-x

Nassar, T., Bdeir, K., Yarovoi, S., Fanne, R. A., Murciano, J.-C., Idell, S., Allen, T. C., Cines, D. B., & Higazi, A. A.-R. (2011). tPA regulates pulmonary vascular activity through NMDA receptors. *American Journal of Physiology-Lung Cellular and Molecular Physiology*, *301*(3), L307–L314. https://doi.org/10.1152/ajplung.00429.2010

National Center for Biotechnology Information. (2024) *PubChem Fluorescein Salt.* https://pubchem.ncbi.nlm.nih.gov/compound/Fluorescein-_sodium-salt

National Center for Biotechnology Information. (2024) *PubChem Muscimol.* https://pubchem.ncbi.nlm.nih.gov/compound/Muscimol

Obeidat, A. S., Jarvis, C. R., & Andrew, R. D. (2000). Glutamate Does Not Mediate Acute Neuronal Damage after Spreading Depression Induced by O_2 /Glucose Deprivation in the Hippocampal Slice. *Journal of Cerebral Blood Flow & Metabolism*, *20*(2), 412–422. https://doi.org/10.1097/00004647-200002000-00024

Proteintech. (2024) *Mouse-on-mouse for Immunohistochemistry: tips and tricks*. https://www.ptglab.com/news/blog/mouse-on-mouse-for-immunohistochemistry-tips-and-tricks/

Rahman, F. A., & Krause, M. P. (2020). PAI-1, the Plasminogen System, and Skeletal Muscle. *International Journal of Molecular Sciences*, *21*(19), 7066. https://doi.org/10.3390/ijms21197066

Reeson, P., Schager, B., Van Sprengel, M., & Brown, C. E. (2022). Behavioral and Neural Activity-Dependent Recanalization of Plugged Capillaries in the Brain of Adult and Aged Mice. *Frontiers in Cellular Neuroscience*, *16*, 876746. https://doi.org/10.3389/fncel.2022.876746

Ribo, M., Montaner, J., Molina, C. A., Arenillas, J. F., Santamarina, E., Quintana, M., & Alvarez-Sabín, J. (2004). Admission Fibrinolytic Profile Is Associated with Symptomatic Hemorrhagic Transformation in Stroke Patients Treated With Tissue Plasminogen Activator. *Stroke*, *35*(9), 2123–2127. https://doi.org/10.1161/01.STR.0000137608.73660.4c

Saver, J. L. (2006). Time Is Brain—Quantified. *Stroke*, *37*(1), 263–266. https://doi.org/10.1161/01.STR.0000196957.55928.ab

Sillen, M., & Declerck, P. J. (2021). A Narrative Review on Plasminogen Activator Inhibitor-1 and Its (Patho)Physiological Role: To Target or Not to Target? *International Journal of Molecular Sciences*, *22*(5), 2721. https://doi.org/10.3390/ijms22052721

Soeda, S., Koyanagi, S., Kuramoto, Y., Kimura, M., Oda, M., Kozako, T., Hayashida, S., & Shimeno, H. (2008). Anti-apoptotic roles of plasminogen activator inhibitor-1 as a neurotrophic factor in

the central nervous system. *Thrombosis and Haemostasis*, *100*(12), 1014–1020. https://doi.org/10.1160/TH08-04-0259

Sweetnam, D., Holmes, A., Tennant, K. A., Zamani, A., Walle, M., Jones, P., Wong, C., & Brown, C. E. (2012). Diabetes Impairs Cortical Plasticity and Functional Recovery Following Ischemic Stroke. *The Journal of Neuroscience*, *32*(15), 5132–5143. https://doi.org/10.1523/JNEUROSCI.5075-11.2012

The National Institute of Neurological Disorders and Stroke rt-PA Stroke Study Group. (1995). Tissue Plasminogen Activator for Acute Ischemic Stroke. *New England Journal of Medicine*, *333*(24), 1581–1588. https://doi.org/10.1056/NEJM199512143332401

Tsao, C. W., Aday, A. W., Almarzooq, Z. I., Anderson, C. A. M., Arora, P., Avery, C. L., Baker-Smith, C. M., Beaton, A. Z., Boehme, A. K., Buxton, A. E., Commodore-Mensah, Y., Elkind, M. S. V., Evenson, K. R., Eze-Nliam, C., Fugar, S., Generoso, G., Heard, D. G., Hiremath, S., Ho, J. E., … on behalf of the American Heart Association Council on Epidemiology and Prevention Statistics Committee and Stroke Statistics Subcommittee. (2023). Heart Disease and Stroke Statistics—2023 Update: A Report From the American Heart Association. *Circulation*, *147*(8). https://doi.org/10.1161/CIR.0000000000001123

Vaughan, D. E., Lazos, S. A., & Tong, K. (1995). Angiotensin II regulates the expression of plasminogen activator inhibitor-1 in cultured endothelial cells. A potential link between the renin-angiotensin system and thrombosis. *Journal of Clinical Investigation*, *95*(3), 995–1001. https://doi.org/10.1172/JCI117809

Watts, L., Zheng, W., Garling, R. J., Frohlich, V. C., & Lechleiter, J. D. (2015). Rose Bengal Photothrombosis by Confocal Optical Imaging In Vivo: A Model of Single Vessel Stroke. *Journal of Visualized Experiments*, *100*, 52794. https://doi.org/10.3791/52794

Appendices

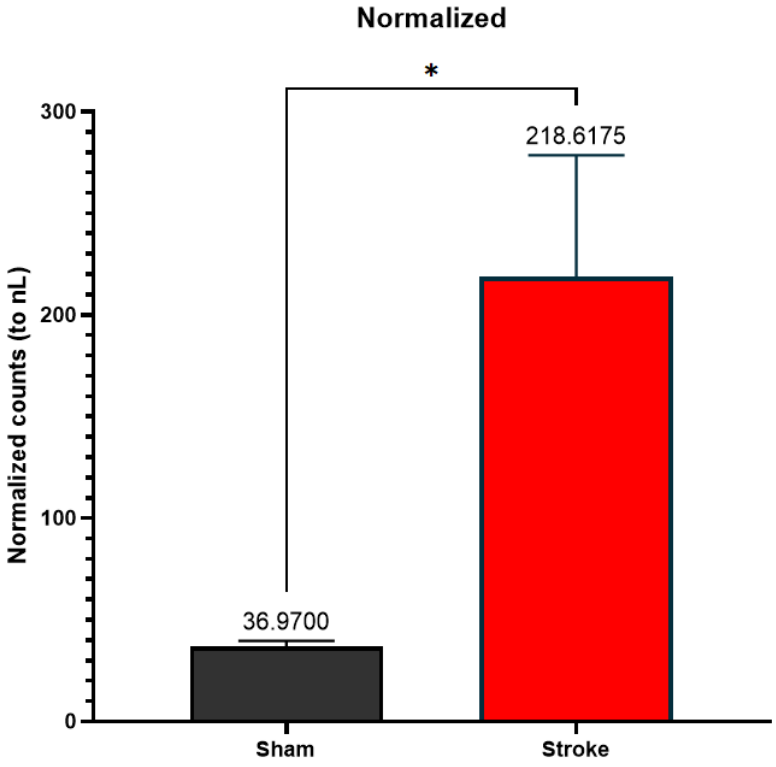

Supplementary Figure 1. Comparison of mature *Serpine1* RNA concentration, indicating translation to PAI-1, following sham or real stroke. Result taken from the stroke affected hemisphere of the brain. An unpaired t-test was conducted (P =.023, n=4). * = P < .05.

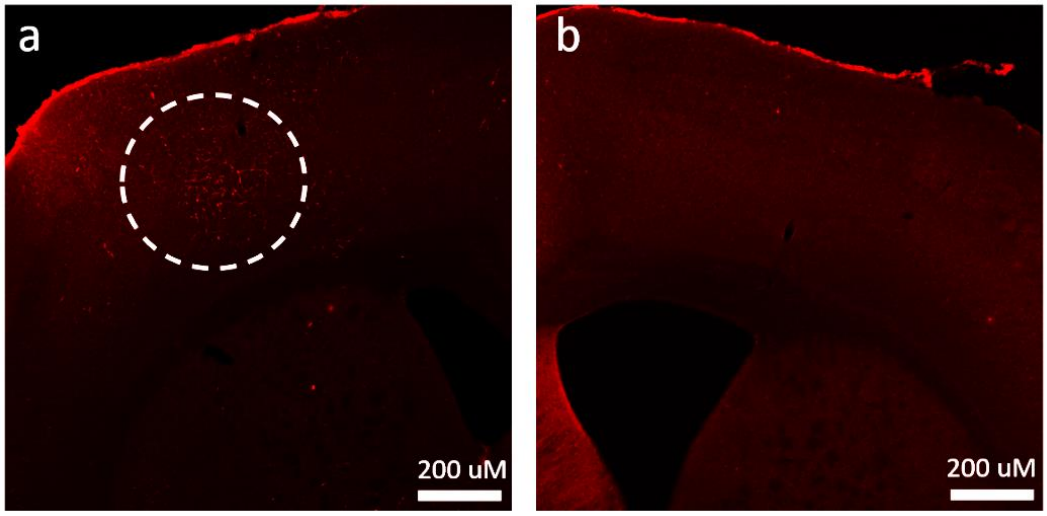

Supplementary Figure 2. Comparison of PAI-1 fluorescence following cerebral microbleed. **a)** Image of primary somatosensory cortex following cerebral microbleed. Small local expression of fluorescence highlighted by white circle. **b)** Comparative image of cortex without cerebral microbleed.

Appendix 1. PAI-1 Immunolabelling Protocol

1) Perfusion and Extraction followed by,
2) Fix tissue in 4% PFA overnight (15-18 hours), then 30% sucrose
3) Rinse PFA fixed brain sections in 0.1M PBS for 2 min
4) Put sections into 1.4mL of sodium citrate buffer (10mM, pH=6.0) in Eppendorf tubes and immerse in water bath for 30min at 75ºC
5) Let tubes rest on bench till it reaches room temp
6) Wash in 0.1M PBS (1 x 5 min)
7) Incubate in primary mouse PAI-1 (1:1000) in PBS+0.2% TX-100 overnight at 4ºC (Overnight without primary antibody for 'no primary' condition).
8) Wash in PBS (3 x 5 min)
9) Incubate in secondary Cy5 anti-mouse (1:500 each) in PBS for 4 hours at room temp
10) Wash in PBS (2 x 5 min)
11) Wash in PBS (2 x 5 min)
12) Mount sections on slides and coverslip with Fluoromount G

Appendix 2. ICAM/VCAM Immunolabelling Protocol

1) Cut the brain using freezing microtome at 50µm thickness.
2) Wash sections in 0.1 M PBS for 10 minutes.
3) Incubate sections overnight at room temperature with ICAM primary antibody (1:200) (Purified Rat anti-mouse CD54 Antibody (ICAM-1); Clone: YN1/1.7.4; Biolegend; Catalogue# 116101; Host Species: Rat) OR VCAM primary antibody (1:200) (Purified Rat anti-mouse CD106 Antibody (VCAM-1); Clone: 429; Biolegend; Catalogue# 105701; Host Species: Rat) in 0.1% TX-100 in PBS. (Overnight without primary antibody for 'no primary' condition).
4) Wash sections in 0.1 M PBS three times (5mins/wash).
5) Incubate in Cy5 conjugated goat secondary anti-rat IgG (1:500 in 0.1M PBS) at room temperature for 4 hours. Remember to spin the secondary antibody briefly before using.
6) Wash in 0.1M PBS two times (5mins/wash).
7) Mount sections on Gelatin slides, dry and coverslip with Fluoromount-G and store in fridge.

Appendix 3. Confocal Imaging and Fluorescence analysis for Immunolabelled images

1) Images of coronal slices taken on a 20x objective lens.
2) Z-stacks performed with 2µm steps, Kalman Filter 1024x1024 pixel resolution.
3) Analyze images in ImageJ FIJI
    a. Z-projection (max intensity)
    b. Duplicate, Median Filter 50 pixels, Subtract median blur image from initial image
    c. Median filter 1.5 pixels
    d. Set threshold (Triangle for VCAM/ICAM, OTSU for PAI-1)
    e. Median filter 1.5 pixels
    f. Set scale to pixels
    g. Pixels above threshold/total pixels x 100 = final expression %

Appendix 4. IgG Blocking Antibody Protocol

Following step 6 of Appendix 1

1) Incubate in Anti-mouse IgG F(ab) Specific (1:100) in PBS+0.2% TX-100 for 6 hours at room temp
2) Wash in PBS (3x5 min)

Appendix 5. Statistical analysis of IgG Blocking experiment

Column B	No Primary + IgG F(ab)		No Primary	No Primary + IgG F(ab)
vs.	vs.		2.34	2.11
Column A	No Primary		1.01	
			1.54	
Paired t test			0.99	
P value		0.5718	1.13	3.16
P value summary	ns		0.45	
Significantly different	No			
One- or two-tailed P \	Two-tailed			
t, df	t=0.7965, df=1			
Number of pairs		2		

Appendix 6. Statistical analysis of ICAM and VCAM Experiments

No Primary vs ICAM PI vs VCAM

Number of families		1								
Number of comparisons per family		3								
Alpha		0.05								
Uncorrected Fisher's LSD	Mean Diff.	95.00% CI of diff.		Below threshold?	Summary	Individual P Value				
No Primary vs. ICAM PI		-2.89	-4.063 to -1.716	Yes	***	0.0002	A-B			
No Primary vs. VCAM		0.1154	-1.058 to 1.289	No	ns	0.834	A-C			
ICAM PI vs. VCAM		3.005	1.832 to 4.178	Yes	***	0.0001	B-C			
Test details	Mean 1	Mean 2		Mean Diff.	SE of diff.	n1	n2	t	DF	
No Primary vs. ICAM PI		0.617	3.507	-2.89	0.5386	5	5	5.366	12	
No Primary vs. VCAM		0.617	0.5016	0.1154	0.5386	5	5	0.2142	12	
ICAM PI vs. VCAM		3.507	0.5016	3.005	0.5386	5	5	5.58	12	
Compact letter display										
ICAM PI	A									
No Primary	B									
VCAM	B									
No Primary	ICAM PI	VCAM								
0.817204	4.523765501	0.528240204								
1.491947	5.318593363	0.782871246								
0.093729	2.423341186	0.231552124								
0.406361	2.995641634	0.608243712								
0.275847	2.272174849	0.357314656								

Sham vs Stroke

Table Analyzed	Data 4		Sham	Stroke
			0.811197	4.523766
Column B	Stroke		0.882359	5.318593
vs.	vs.		0.519967	2.423341
Column A	Sham		1.094847	2.995642
				2.272175
Unpaired t test				
P value		0.0061		
P value summary	**			
Significantly different (P < 0.05)?	Yes			
One- or two-tailed P value?	Two-tailed			
t, df	t=3.873, df=7			

No Muscimol vs Stroke + No Muscimol vs Muscimol vs Stroke + Muscimol

Number of families	1
Number of comparisons per family	6
Alpha	0.05

Tukey's multiple comparisons test	Mean Diff.	95.00% CI of diff.	Below threshold?	Summary	Adjusted P Value	
No Muscimol vs. Muscimol	-0.4581	-3.214 to 2.298	No	ns	0.9236	A-B
No Muscimol vs. No Muscimol +Stroke	-1.083	-3.599 to 1.433	No	ns	0.4598	A-C
No Muscimol vs. Muscimol +Stroke	-0.8891	-3.645 to 1.867	No	ns	0.6576	A-D
Muscimol vs. No Muscimol +Stroke	-0.6248	-3.140 to 1.891	No	ns	0.7982	B-C
Muscimol vs. Muscimol +Stroke	-0.431	-3.187 to 2.325	No	ns	0.9348	B-D
No Muscimol +Stroke vs. Muscimol +Stroke	0.1938	-2.322 to 2.709	No	ns	0.991	C-D

Test details	Mean 1	Mean 2	Mean Diff.	SE of diff.	n1	n2	q	DF
No Muscimol vs. Muscimol	0.714	1.172	-0.4581	0.7468	2	2	0.8674	5
No Muscimol vs. No Muscimol +Stroke	0.714	1.797	-1.083	0.6818	2	3	2.246	5
No Muscimol vs. Muscimol +Stroke	0.714	1.603	-0.8891	0.7468	2	2	1.684	5
Muscimol vs. No Muscimol +Stroke	1.172	1.797	-0.6248	0.6818	2	3	1.296	5
Muscimol vs. Muscimol +Stroke	1.172	1.603	-0.431	0.7468	2	2	0.8161	5
No Muscimol +Stroke vs. Muscimol +Stroke	1.797	1.603	0.1938	0.6818	3	2	0.402	5

Compact letter display		No Muscimol	Muscimol	No Muscimol + Stroke	Muscimol + Stroke
No Muscimol +Stroke	A	0.871065	1.784421	1.453523	2.512246
Muscimol +Stroke	A	0.557018	0.559805	1.686061	0.693939
Muscimol	A			2.251135	
No Muscimol	A				

Regional Comparison of ICAM

Number of families	1
Number of comparisons per family	10
Alpha	0.05

Tukey's multiple comparisons test	Mean Diff.	95.00% CI of diff.	Below threshold?	Summary	Adjusted P Value	
PI Medial vs. PI Lateral	0.3108	-2.596 to 3.218	No	ns	0.9962	A-B
PI Medial vs. SS2	2.308	-0.5992 to 5.214	No	ns	0.141	A-C
PI Medial vs. CL	2.447	-0.4597 to 5.354	No	ns	0.1113	A-D
PI Medial vs. CL SS2	2.749	-0.1576 to 5.656	No	ns	0.0659	A-E
PI Lateral vs. SS2	1.997	-0.9100 to 4.904	No	ns	0.234	B-C
PI Lateral vs. CL	2.136	-0.7706 to 5.043	No	ns	0.1872	B-D
PI Lateral vs. CL SS2	2.438	-0.4685 to 5.345	No	ns	0.113	B-E
SS2 vs. CL	0.1394	-2.767 to 3.046	No	ns	0.9998	C-D
SS2 vs. CL SS2	0.4415	-2.465 to 3.348	No	ns	0.9855	C-E
CL vs. CL SS2	0.3021	-2.605 to 3.209	No	ns	0.9965	D-E

Test details	Mean 1	Mean 2	Mean Diff.	SE of diff.	n1	n2	q	DF
PI Medial vs. PI Lateral	4.244	3.933	0.3108	0.8832	3	3	0.4977	10
PI Medial vs. SS2	4.244	1.936	2.308	0.8832	3	3	3.695	10
PI Medial vs. CL	4.244	1.797	2.447	0.8832	3	3	3.918	10
PI Medial vs. CL SS2	4.244	1.495	2.749	0.8832	3	3	4.402	10
PI Lateral vs. SS2	3.933	1.936	1.997	0.8832	3	3	3.197	10
PI Lateral vs. CL	3.933	1.797	2.136	0.8832	3	3	3.42	10
PI Lateral vs. CL SS2	3.933	1.495	2.438	0.8832	3	3	3.904	10
SS2 vs. CL	1.936	1.797	0.1394	0.8832	3	3	0.2233	10
SS2 vs. CL SS2	1.936	1.495	0.4415	0.8832	3	3	0.707	10
CL vs. CL SS2	1.797	1.495	0.3021	0.8832	3	3	0.4837	10

Compact letter display

		PI Medial	PI Lateral	SS2	CL	CL SS2
PI Medial	A					
PI Lateral	A	4.557823	4.489707947	1.067448	2.251134644	1.185282
SS2	A	5.873697	4.76349019	1.808482	1.453522797	1.617393
CL	A	2.300403	2.54627961	2.933081	1.686061182	1.681741
CL SS2	A					